Synthesis of Water-Soluble $CuInS_2$ Quantum Dots by a Hydrothermal Method and Their Optical Properties

Kazutaka Iida, Yota Uehigashi, Hideki Ichida, Hang-Beom Bu, and DaeGwi Kim

Citation	Bulletin of the Chemical Society of Japan. 92(5); 930-936
Issue Date	2019-02-13
Type	Journal Article
Textversion	Author
Rights	© 2019 The Chemical Society of Japan. The following article has been accepted by Bulletin of the Chemical Society of Japan. After it is published, it will be found at https://doi.org/10.1246/bcsj.20180399.
Supporting Information	Supporting Information is available at online: https://doi.org/10.1246/bcsj.20180399.
DOI	10.1246/bcsj.20180399

IIDA K., UEHIGASHI Y., BU H.-B., KIM D., ICHIDA H., & BU H.-B. (2019). Synthesis of water-soluble $CuInS_2$ quantum dots by a hydrothermal method and their optical properties. *Bulletin of the Chemical Society of Japan*. 92, 930-936. doi:10.1246/bcsj.20180399

Synthesis of water-soluble $CuInS_2$ quantum dots by a hydrothermal method and their optical properties

Kazutaka Iida,[1] Yota Uehigashi,[1] Hideki Ichida,[2] Hang-Beom Bu,[1,3] and DaeGwi Kim*[1]

[1]Department of Applied Physics, Osaka City University, Osaka 558-8585, Japan

[2]Faculty of Engineering, Nippon Bunri University, Oita 870-0397, Japan

[3]*Nano Earth*, 1-5-20 Kashitanishi, Higashiosaka, Osaka 577-0835, Japan

E-mail: <tegi@a-phys.eng.osaka-cu.ac.jp >

DaeGwi Kim
DaeGwi Kim graduated from Korea University and received Ph.D. degree from Osaka City University in 1997. He began his academic career at OCU as an Assistant Professor, and was promoted to Professor at OCU in 2012. His research interests are in synthesis and optical properties of semiconductor nanomaterials.

Abstract

Water-soluble $CuInS_2$ (CIS) quantum dots (QDs) were hydrothermally prepared in the presence of *N*-acetyl-*L*-cysteine (NAC) as a stabilizer, and the optimal hydrothermal synthetic conditions for NAC-capped CIS QDs were investigated. The photoluminescence (PL) quantum yield (QY) of the CIS QDs synthesized under optimal conditions was 4%, which was comparable with the highest QY reported for water-soluble CIS core QDs. The introduction of a ZnS shell produced CIS/ZnS core/shell QDs and further increased the PL QY to 30%. Furthermore, bilayer structures consisting of Au nanoparticles and CIS/ZnS QDs were fabricated using a layer-by-layer method to enhance the PL of the CIS/ZnS QDs on the basis of the localized surface plasmon resonance of Au nanoparticles.

1. Introduction

Electrons and/or excitons are three-dimensionally confined in semiconductor quantum dots (QDs), thus resulting in the quantum size effect.[1–4] Consequently, semiconductor QDs exhibit optical properties that are different from bulk crystals. For example, the absorption and photoluminescence (PL) energies of QDs can be controlled by changing the QD size, and QDs have high PL quantum yields (QYs) even at room temperature.[5–8] QDs have been extensively studied for use in various applications, including light-emitting diodes,[9] biomolecular imaging,[10] and QD solar cells.[11]

To date, most studies have focused on the QDs of type II–VI semiconductors such as CdTe, CdSe, and CdS,[12–16] with a particular focus on CdSe QDs with uniform size and high PL QY.[12,14,15] However, these semiconductor QDs contain the toxic element Cd, and their application in consumer products is strictly regulated. $CuInS_2$ (CIS) QDs have recently attracted considerable attention as Cd-free QDs. CIS is a direct transition-type semiconductor with a band-gap energy of 1.5 eV and a high absorption coefficient ($\alpha \geq 10^5$ cm^{-1}).[17] Furthermore, CIS QDs are expected to find applications in new bioimaging materials because they exhibit PL in the near-infrared region.[17–19]

CIS QDs are most commonly synthesized by a hot-injection method, which relies on a chemical reaction in organic solvent.[18–27] Uehara *et al*. reported the synthesis of CIS and CIS/ZnS core/shell QDs with PL QYs of 5% and 15%, respectively.[28] Li *et al*. successfully synthesized CIS/ZnS and CIS/CdS core/shell QDs with high PL QYs of 67% and 86%, respectively.[29] For applications in bioimaging, the QDs must be water-soluble. Hot injection results in oil-soluble QDs; therefore, ligand exchange is necessary to disperse the QDs in water. However, ligand exchange is known to decrease the PL intensity of QDs.[18,19,30] Therefore, a method for the direct synthesis of water-soluble CIS QDs with good optical properties is still needed.[31–34]

Liu *et al*. synthesized mercaptopropionic acid-capped CIS QDs by using a hydrothermal method and studied the effects of experimental variables such as reaction time, reaction temperature, and pH;[32] the CIS QDs were synthesized at 150 °C for 21 h and exhibited a PL QY of 3%. Chen *et al*. reported the synthesis of CIS QDs by using a reflux method at 95 °C in the presence of *L*-glutathione (GSH) as a ligand.[33] Although the PL QY of the CIS QDs was only 3%, the authors successfully synthesized CIS/ZnS core/shell QDs with a high PL QY of 38%.[33] Compared with conventional thermal techniques, microwave irradiation enables the rapid and efficient synthesis of QDs.[34] For example, Xiong *et al*. used a microwave-assisted approach to synthesize GSH-capped CIS/ZnS QDs with a PL QY of 24% within a reaction time of 10 min.[35]

When synthesizing water-soluble QDs via reflux and/or hydrothermal methods, the ligand selection strongly affects the PL properties and dispersion stability of the resulting QDs. *N*-acetyl-*L*-cysteine (NAC) is a well-known nutritional supplement derived from naturally occurring amino acids. In addition to being nonvolatile and nontoxic, NAC possesses good water solubility and excellent biocompatibility.[36–40] To date, NAC-capped CdTe/CdS,[36,37] CdTe,[37,38] and ZnSe QDs,[39,40] have been successfully synthesized with excellent PL properties. Therefore, NAC shows great potential for use as a ligand in the synthesis of water-soluble CIS QDs.

Bu *et al*. reported the synthesis of NAC-capped CIS QDs;[41] however, the PL QY was very low (<1%). In this study, we attempted to improve the PL characteristics of NAC-capped CIS QDs by optimizing the synthetic conditions, including the In/Cu molar ratio, S/(Cu+In) ratio, (Cu+In)/NAC ratio, and reaction temperature. The CIS QDs prepared using the optimized synthetic conditions exhibited an improved PL QY of 4%. A high PL QY of 30% was obtained by preparing CIS/ZnS core/shell QDs. A layer-by-layer (LBL) method was then applied to prepare bilayer structures consisting of Au nanoparticles (NPs) and CIS/ZnS QDs. The PL intensity of the CIS/ZnS QDs in the bilayer structure was enhanced by a factor

of two on the basis of the localized surface plasmon resonance (LSPR) of the Au NPs.

2. Experimental

2.1 Sample Preparation: $CuCl_2·2H_2O$, $Na_2S·9H_2O$, and aqueous ammonia (28%) were purchased from Kishida Chamical. $InCl_3·4H_2O$ and NAC were obtained from Kanto Chemical. All chemicals were used as received without further purification. Deionized (DI) water was purged with N_2 gas for 30 min before use. Au NPs with diameters of 23 nm were purchased from Tokuriki Chemical Research (Japan).

CIS QDs were synthesized hydrothermally as follows. First, a precursor solution was prepared in accordance with the procedure reported in Ref. [41]. Equal amounts of NAC (2.4 mmol) were added to two glass vessels containing 50 mL DI water, and $CuCl_2·2H_2O$ (0.4 mmol) and $InCl_3·4H_2O$ (0.4 mmol) were added. After mixing the two solutions, a dilute ammonia solution was added to adjust the pH to 3.0. Subsequently, 8 mL of $Na_2S·9H_2O$ (0.1 M) solution was added to prepare the precursor solutions of CIS. Finally, 10 mL of the precursor solution was loaded into an autoclave and incubated in an oven at varying temperatures for specified periods. To determine the optimal conditions, various precursor solutions were prepared with different molar ratios of Cu:In:S:NAC.

To improve the PL QY, we synthesized CIS/ZnS core/shell QDs. First, ZnS precursor solution was prepared as follows. $Zn(ClO_4)_2·6H_2O$ (0.53 mmol) and NAC (2.54 mmol) were dissolved in 20 mL DI water, and the pH was adjusted to 5.0. After adding $Na_2S·9H_2O$ (0.16 mmol), the precursor solution was adjusted to pH 6.0. The ZnS precursor solution was added to the already prepared CIS QD solution, and CIS/ZnS core/shell QDs were synthesized under microwave irradiation.

To enhance the PL of the CIS/ZnS QDs on the basis of the LSPR of Au NPs, bilayer structures consisting of Au NPs and CIS/ZnS QDs were fabricated using a LBL method.[42] The bilayer structures were composed of three main blocks: a monolayer of Au NPs; a poly(diallyldimethylammonium chloride) (PDDA) and poly(acrylic acid) (PAA) spacer layer with structure PDDA/$(PAA/PDDA)_n$, where the notation $(PAA/PDDA)_n$ represents n bilayers of PAA and PDDA; and a monolayer of CIS/ZnS QDs. Therefore, the structure of the bilayer was (Au NPs)/[PDDA/$(PAA/PDDA)_n$]/(CIS/ZnS QDs).

2.2 Characterization and Spectroscopic Measurements: X-ray diffraction (XRD) measurements were performed on a Rigaku SmartLab diffractometer with Cu Kα radiation. Transmission electron microscopy (TEM) images were obtained using a JEOL JEM-2100 microscope. The monolayer structures of CIS and CIS/ZnS QDs were prepared for X-ray photoelectron spectroscopy (XPS) measurements as follows. Si substrates were cleaned by immersion in fresh piranha solution (1/3 [v/v] mixture of 30% H_2O_2 and 98% H_2SO_4) for 20 min. The substrates were then rinsed with water and used immediately after cleaning. Thereafter, a polyelectrolyte adhesion layer consisting of positively charged PDDA was deposited to enhance the QD binding. The monolayer structures of CIS and CIS/ZnS QDs were then deposited onto the PDDA layer.

A JASCO V-650 UV/Vis spectrophotometer and a JASCO FP-8300 spectrofluorometer were used to record the absorption and PL spectra, respectively. The excitation wavelength was fixed at 405 nm. The PL intensity of each sample was compared by dividing the PL intensity by the absorption intensity at the excitation wavelength. PL QYs were measured with an absolute PL measurement system (Hamamatsu, CQQ20). A laser diode (405 nm; Hamamatsu PLP M10-040) with a pulse duration of 100 ps and a repetition rate of 100 kHz was used as the excitation light to measure the PL decay profiles. A time-correlated single-photon counting method was used to obtain the decay profiles.

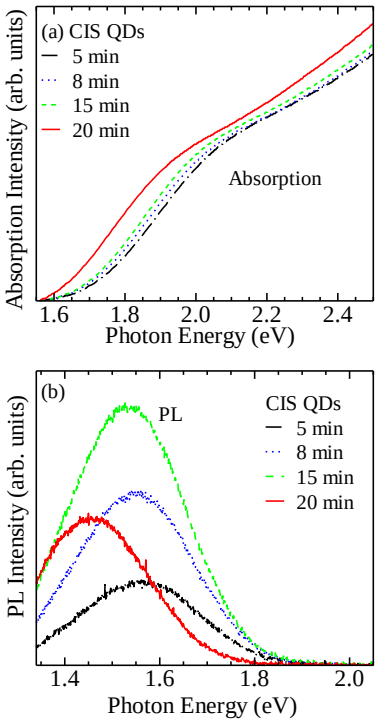

Fig. 1. (a) Absorption and (b) PL spectra of CIS QDs synthesized with Cu:In:S = 1:1:2 at 180 °C and reaction times of 5, 8, 15, and 20 min.

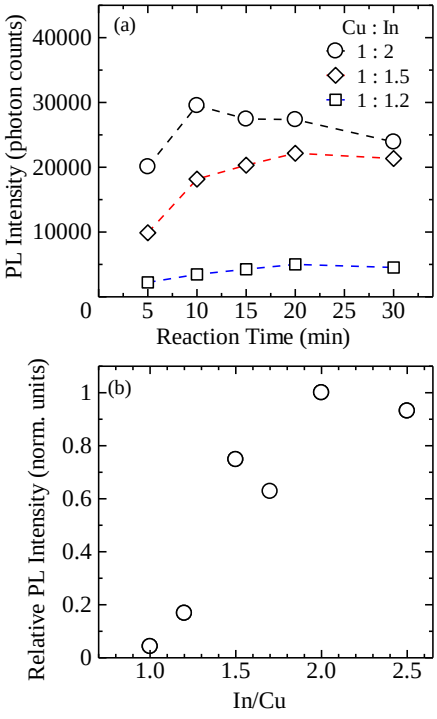

Fig. 2. (a) PL intensity of CIS QDs synthesized with In/Cu = 1.2, 1.5, and 2.0 as a function of reaction time. (b) Dependence of the relative PL intensity of CIS QDs on the In/Cu molar ratio.

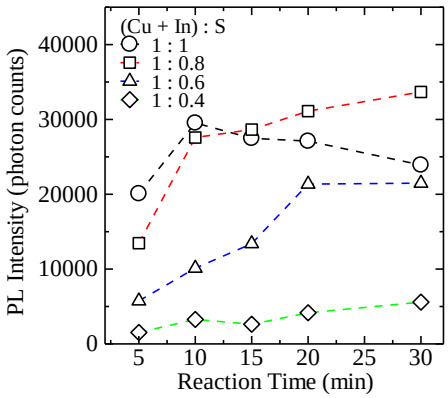

Fig. 3. PL intensity of CIS QDs synthesized with S/(Cu+In) = 0.4, 0.6, 0.8, and 1.0 as a function of reaction time. The In/Cu molar ratio was fixed at 2.0.

3. Results and Discussion.

Figure 1 shows the absorption and PL spectra of the CIS QDs synthesized with Cu, In, and S at a ratio of 1:1:2. The reactions were performed at 180 °C for 5, 8, 15, or 20 min to generate QDs with different mean sizes. The absorption and PL energies of the QDs decreased with increasing reaction time, thus indicating that QD mean size increased with increasing reaction time. The PL intensity of the CIS QDs was maximized at a reaction time of 15 min. However, the PL QY was very low (<1%).

During the synthesis of CIS QDs, the In/Cu molar ratio is known to strongly affect the PL intensity of the resulting QDs.[28,33,43] Few studies have investigated the effect of the In/Cu molar ratio on the synthesis of NAC-capped CIS QDs. To maximize PL QY, we prepared CIS QDs from precursor solutions with different In/Cu molar ratios with (Cu+In)/S = 1. Figure 2(a) shows the PL intensities of the CIS QDs synthesized from three different In/Cu molar ratios as a function of reaction time. No PL was observed for the CIS QDs synthesized with In/Cu < 1. The PL intensity of each sample varied with reaction time, and this result is in agreement with the results shown in Fig. 1. As reported previously,[28,33,43] the PL intensity of the NAC-capped CIS QDs depended strongly on the In/Cu molar ratio in this study. The maximum PL intensity achieved in each sample is shown in Fig. 2(b), which plots the PL intensity relative to that of the CIS QDs synthesized with In/Cu = 1.0. The PL intensity of the CIS QDs increased with increasing In/Cu molar ratio and was maximized at In/Cu = 2.0. The PL intensity obtained at In/Cu = 2.0 was 23 times that achieved at In/Cu = 1.0.

We then discussed the effect of the S/(Cu+In) molar ratio on the PL intensity of CIS QDs. Although some studies have investigated the effect of the In/Cu molar ratio on the PL intensity of CIS QDs, few studies have focused on the effect of the S/(Cu+In) molar ratio. We synthesized CIS QDs with various S/(Cu+In) molar ratios in the range of 0.3–2.0. No PL was observed in the CIS QDs synthesized with S/(Cu+In) > 1. Figure 3 shows the PL intensity of the CIS QDs synthesized with S/(Cu+In) = 0.4, 0.6, 0.8, and 1.0 as a function of reaction time. In all cases, the In/Cu molar ratio was fixed at 2.0. The S/(Cu+In) molar ratio clearly had a strong influence on the PL characteristics of the CIS QDs. The PL intensity of the CIS QDs decreased greatly when S/(Cu+In) < 0.8. At a reaction time of 15 min or less, the difference in PL between the CIS QDs synthesized with S/(Cu+In) = 0.8 and 1.0 was not obvious. However, for S/(Cu+In) = 0.8, the PL intensity increased with increasing reaction time, whereas the PL for S/(Cu+In) = 1.0 decreased. Therefore, the optimum S/(Cu+In) molar ratio was

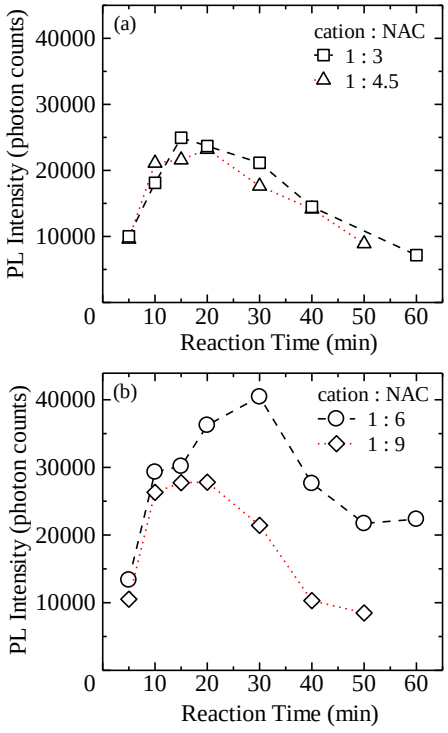

Fig. 4. PL intensity of CIS QDs synthesized with NAC/(Cu+In) = 3.0, 4.5, 6.0, and 9.0 as a function of reaction time. The Cu:In:S molar ratio was fixed at the optimum value of 1:2:2.4.

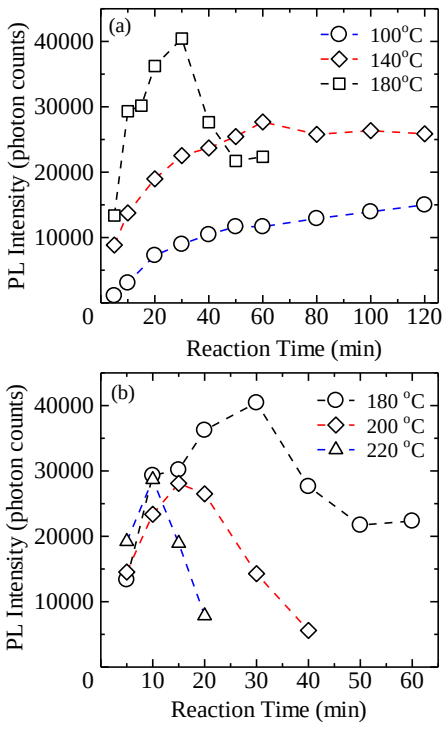

Fig. 5. PL intensity of CIS QDs synthesized at five reaction temperatures as a function of reaction time. The precursor solutions were prepared with the optimum Cu:In:S:NAC ratio of 1:2:2.4:18.

determined to be 0.8.

As reported in Refs. [18], [21], [32], and [35], the molar ratio of ligand to cation is also an important factor when synthesizing CIS QDs. Figure 4 shows the PL intensity of CIS QDs synthesized with NAC/(Cu+In) = 3.0, 4.5, 6.0, and 9.0 as a function of reaction time. The molar ratio of Cu, In, and S was fixed at the optimum value of 1:2:2.4. Although the reaction time dependence was similar for each sample, the PL intensity was the highest in the CIS QDs synthesized with NAC/(Cu+In) = 6.0. Therefore, NAC/(Cu+In) = 6.0 was selected as the optimal ligand–cation molar ratio.

Finally, we optimized the reaction temperature during the synthesis of NAC-capped CIS QDs. Figure 5 shows the PL intensity of CIS QDs synthesized at five different reaction temperatures as a function of reaction time. The precursor solutions were prepared with the optimum Cu:In:S:NAC ratio of 1:2:2.4:18. The PL intensity varied greatly with reaction temperature. The PL intensity first increased with reaction temperature until 180 ℃ and then decreased with further increasing temperature. QDs began to precipitate after 60 min at 180 °C, after 40 min at 200 °C, and after 20 min at 220 °C. This phenomenon is attributed to the thermal decomposition of the NAC ligand [36, 37]. The results indicate that the optimum reaction temperature was 180 °C and that the PL intensity of the QDs synthesized at 180 °C was maximized after 30 min of reaction time. The PL QY of the CIS QDs prepared under the optimized conditions (Cu:In:S:NAC = 1:2:2.4:18, reaction temperature = 180 °C, and reaction time = 30 min) was 4%. To the best of our knowledge, this PL QY is comparable to the highest value reported for water-soluble CIS core QDs.

Figure 6(a) shows a typical XRD pattern of CIS QDs. The XRD pattern shows three broad but distinct peaks corresponding to the (112), (204)/(320), and (116)/(312) planes of the chalcopyrite CIS lattice structure, thus demonstrating that CIS QDs were successfully formed. Figure 6(b) shows a TEM image of the CIS QDs. The mean diameter of the CIS QDs of 5.4 nm was estimated from this TEM image.

The preparation of core/shell QDs greatly improves the PL properties of QDs. ZnS, which is a wide-gap semiconductor, is the most commonly used shell material because of the

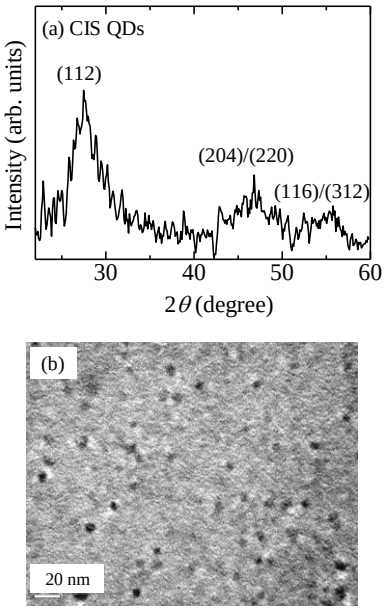

Fig. 6. (a) XRD pattern and (b) TEM image of CIS QDs.

following reasons: (1) ZnS shell layers can be epitaxially grown on CIS QDs because the lattice mismatch between CIS and ZnS is approximately 2%–3%.[17] (2) ZnS does not contain toxic elements. (3) Given that CIS/ZnS QDs are type I QDs in which electrons and holes are confined in the core, the ZnS shell suppresses the nonradiative recombination rate at the surface, thereby increasing the PL intensity. Thus, CIS/ZnS core/shell QDs were prepared to further increase the PL QY of the NAC-capped CIS QDs.

The XPS spectra of the CIS QDs and CIS/ZnS core/shell QDs were measured to evaluate the differences in their surface compositions. Figure 7 shows the Cu 2p (a), In 3d (b), and S 2p (c) XPS spectra of the CIS QDs (solid curves) and CIS/ZnS core/shell QDs (broken curves). The signal intensities in the Cu 2p and In 3d spectra of the CIS/ZnS QDs are significantly lower than those in the CIS QDs spectra; by contrast, the intensities in the S 2p spectra were similar for the CIS and

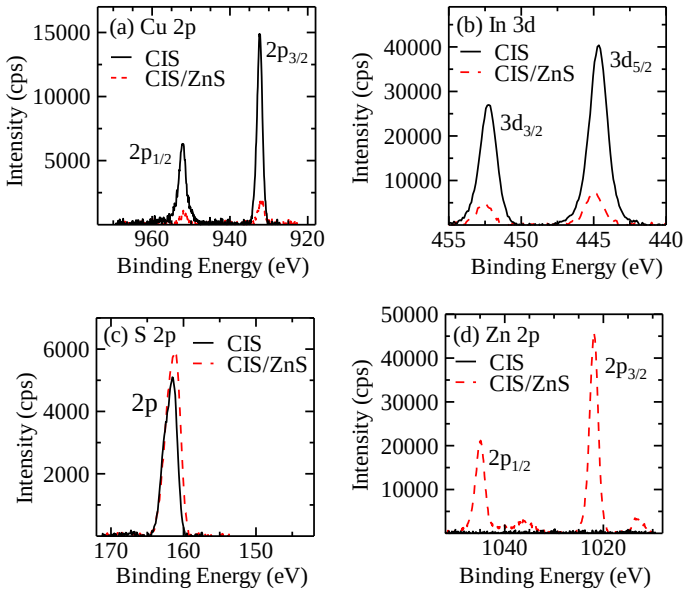

Fig. 7. (a) Cu 2p, (b) In 3d, (c) S 2P, and (d) Zn 2p XPS spectra of CIS core QDs (solid curves) and CIS/ZnS core/shell QDs (broken curves).

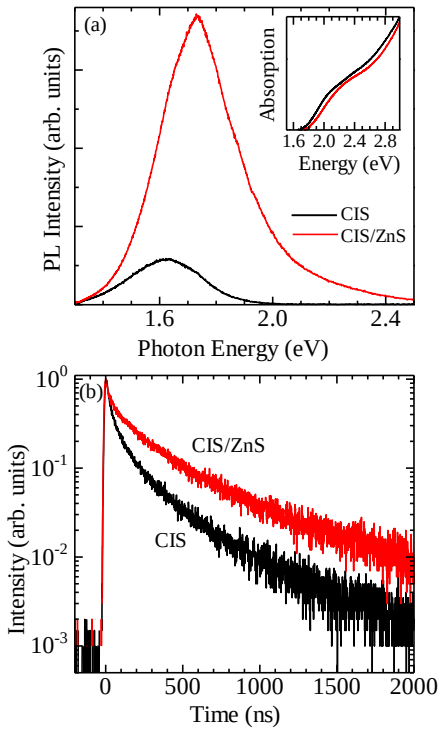

Fig. 8. (a) PL spectra and (b) PL decay profiles of CIS and CIS/ZnS QDs. The inset shows the absorption spectra of the CIS and CIS/ZnS QDs.

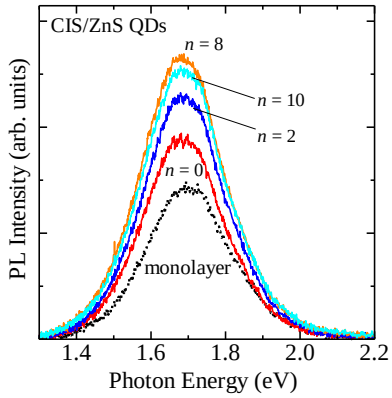

Fig. 9. PL spectra of bilayer structures of (Au NPs)/[PDDA/(PAA/PDDA)$_n$]/(CIS/ZnS QDs) structures with n = 0, 2, 6, 8, and 10. The broken curve corresponds to the PL spectrum of the monolayer CIS/ZnS QD structure as a control.

CIS/ZnS QDs. The Zn 2p signal was clearly observed in the CIS/ZnS QD spectrum (Fig. 7[d]). These XPS results clearly demonstrate the presence of the ZnS shell in the CIS/ZnS QDs.

Figure 8(a) shows the PL spectra of the CIS and CIS/ZnS QDs. The addition of the ZnS shell caused the PL peak to shift toward higher energy. The inset shows the absorption spectra of the CIS and CIS/ZnS QDs. The absorption peak of CIS/ZnS shifts to the higher energy side compared with CIS similarly to the PL peak. Generally, the preparation of core/shell QDs increases the effective confinement size, thus causing the PL energy to shift toward a lower energy value.[44,45] The high-energy shift observed in this study for the CIS/ZnS QDs might be explained by the following:[33] (1) CIS–ZnS alloy formed at the interface, and/or (2) the CIS core QDs were etched during the growth of the ZnS shell layer, thus decreasing the core size.

The PL intensity of the CIZ/ZnS core/shell QDs was seven times greater than that of the CIS QDs. The PL decay profile of the CIS/ZnS QDs was longer than that of the CIS QDs (Fig. 8(b)). These results clearly demonstrate that the formation of the ZnS shell suppressed nonradiative recombination, thus resulting in PL enhancement in the CIS/ZnS QDs. The PL QY of the CIS/ZnS QDs was approximately 30%. Thus, water-soluble CIS/ZnS QDs that are exhibiting high PL QY were successfully prepared.

Finally, we discuss the enhancement of PL in CIS/ZnS QDs on the basis of the LSPR of Au NPs. When semiconductor QDs and metal NPs are close to each other, the PL of the system is enhanced by LSPR, and PL quenching arises from energy transfer from the semiconductor QDs to the metal NPs.[46–51] These effects depend strongly on the distance between the QDs and NPs. Kim *et al*. fabricated layered structures that comprise semiconductor QDs and Au NPs and reported that the interlayer distance is an important factor in PL enhancement.[42] By using LBL assembly, we prepared bilayer structures consisting of Au NP and CIS/ZnS QD monolayers separated by a polyelectrolyte spacer layer: (Au NPs)/[PDDA/(PAA/PDDA)$_n$]/(CIS/ZnS QDs). Figure 9 shows the PL spectra of the bilayer structures of n = 0, 2, 6, 8, and 10. The broken curve in Fig. 9 corresponds to the PL spectrum of the monolayer CIS/ZnS QD structure as a control. The PL intensity was higher in the bilayer structures than in the control sample and increased with increasing spacer layer thickness until n = 8. Further increases in n beyond eight caused the PL intensity to decrease. These results clearly demonstrate that the PL intensity of CIS/ZnS QDs can be enhanced on the basis of the LSPR of Au NPs.

As discussed in Ref. [42], there are two effects for the PL enhancement: the enhancement of the electric field enhancement and of the radiative recombination probability due to localized surface plasmon excitation. In the latter case, the PL-decay time becomes shortened, while that does not change in the former case. Figure S1 shows PL-decay profiles of the monolayer structure of CIS QDs and the bilayer structures of n = 0 and 8. The PL-decay profiles in the bilayer structure with n=0 and 8 are consistent with that in the monolayer structure of the CIS QDs. This result demonstrates that the electric field enhancement due to localized surface plasmons is the dominant effect for the PL enhancement in the present bilayer structure.

4. Conclusion

We determined the optimal conditions for the synthesis of water-soluble CIS QDs. The optimum Cu:In:S:NAC molar ratio for synthesizing NAC-capped CIS QDs was found to be 1.0:2.0:2.4:18. The PL QY of the CIS QDs synthesized under the optimum conditions was 4%, which is comparable with the highest value that has been reported for water-soluble CIS core QDs. The addition of a ZnS shell to the CIS QDs to form CIS/ZnS core/shell QDs increased the PL intensity by seven times compared with the CIS QDs. From the viewpoint of PL dynamics, the addition of the ZnS shell suppressed nonradiative recombination processes to produce the enhancement in PL intensity. The CIS/ZnS QDs exhibited a PL QY of approximately 30%. Finally, the PL intensity of the CIS/ZnS QDs was successfully doubled by taking advantage of the LSPR of Au NPs.

References

1. L. E. Brus, *J. Chem. Phys.* **1984**, *80*, 4403.
2. Y. Kayanuma, *Phys. Rev. B* **1988**, *38*, 9797.
3. L. Brus, *Appl. Phys. A* **1991**, *53*, 465.

4. Y. Wang and N. Herron, *J. Phys. Chem.* **1991**, *95*, 525.
5. D. J. Norris and M. G. Bawendi, *Phys. Rev. B* **1996**, *53*, 16338.
6. D. J. Norris, A. L. Efros, M. Rosen, and M. G. Bawendi, *Phys. Rev. B* **1996**, *53*, 16347.
7. X. michalet, F. F. Pinaud, L. A. Bentolila, J. M. Tsay, S. Doose, J. J. Li, G. Sundaresan, A. M. Wu, S. S. Gambhir, and S. Weiss, *Science* **2005**, *307*, 538.
8. A. P. Alivisatos, *Science* **1996**, *271*, 933.
9. P. O. Anikeeva, J. E. Halpert, M. G. Bawendi, and V. Bulovic, *Nano Lett.* **2009**, *9*, 2532.
10. Y. Zhang, C. Xie, H. Su, J. Liu, S. Pickering, Y. Wang, W. W. Yu, J. Wang, Y. Wang, J. Hahm,N. dellas, S. E. Mohney, and J. Xu, *Nano Lett.* **2011**, *11*, 329.
11. A. J. Nozik, *Physica E* **2002,** *14*, 115.
12. C. B. Murray, D. J. Norris, and M. G. Bawendi, *J. Am. Chem. Soc*. **1993**, *115*, 8706.
13. H. Bu, H. Kikunaga, K. Shimura, K. Takahasi, T. Taniguchi, and D. Kim, *Phys. Chem*. *Chem. Phys.* **2013**, *15*, 2903.
14. D. Kim, H. Yokota, K. Shimura, and M. Nakayama, *Phys. Chem. Chem. Phys.* **2013**, *15*, 21051.
15. J. J. Li, Y. A. Wang, W. Guo, J. C. Keay, T. D. Mishima, M. B. Johnson, and X. Peng, *J. Am. Chem. Soc.* **2003**, *125*, 12567.
16. P. Reiss, *New J. Chem.* **2007**, *31*, 1843.
17. L. Li, T. J. Daou, I. Texier, T. T. Kim Chi, N. Q. Liem and P. Reiss, *Chem. Mater*. **2009**, *21*, 2422.
18. D. Deng, Y. Chen, J. Cao, J. Tian, Z. Qian, S. Achilefu and Y. Gu, *Chem. Mater*. **2012**, *24*, 3029.
19. J. Kolny-Olesiak, and H. Weller, *ACS Appl. Mater. Interfaces* **2013**, *5*, 12221.
20. H. Zhong, Y. Zhou, M. Ye, Y. He, J. Ye, C. He, C. Yang, and Y. Li. *Chem. Mater*. **2008**, *20*, 6435.
21. R. Xie, M. Rutherford, and X. Peng, *J. Am. Chem. Soc*. **2009,** *131*, 5691.
22. T. Pons, E. Pic, N. Lequeux, E. Cassett, L. Bezdetnaya, F. Guillemin, F. Marchal, and B. Dubertret, *ACS Nano*. **2010**, *4*, 2531.
23. H. Kim, J. Y. Han, D. S. Kang, S. W. Kim, D. S. Jang, M. Suh, A. Kirakosyan and D. Y. Jeon, *J. Cryst. Growth* **2011**, *326*, 90.
24. M. Booth, A. P. Brown, S. D. Evans, and K. Critchley, *Chem. Mater*. **2012**, *24*, 2064.
25. M. Oda, T. Miyaoka, S. Yamada, and T. Tani, *Physics Procedia*. **2012**, *29*, 18.
26. W. Song and H. Yang, *Chem. Mater*. **2012**, *24*, 1961.
27. P. Chuang, C. C. Lin and R. Liu, *ACS Appl. Mater. Intefaes* **2014**, *6*, 15379.
28. M. Uehara, K. Watanabe, Y. Tajiri, H. Nakamura, and H. Maeda, *J. Chem. Phys*. **2008**, *129*, 134709.
29. L. Li, A. Pandey, D. J. Werder, B. P. Khanal, J. M. Pietryga, and V. I. Klimov, *J. Am. Chem. Soc*. **2011,** *133*, 1176.
30. L. Liu and X. Zhong, *Chem. Commun*. **2012**, *48*, 5718.
31. F. Bensebaa, C. Durand, A. Aouadou, L. Scoles, X. Du, D. Wang, Y. L. Page, *J. Nanopart. Res*. **2010**, *12*, 1897.
32. S. Liu, H. Zhang, Y. Qiao and X. Su, *RSC Adv*. **2012**, *2*, 819.
33. Y. Chen, S. Li, L. Huang and D. Pan, *Inorg. Chem*. **2013**, *52*, 7819.
34. J. A. Gerbec, D. Magana, A. Washington, G. F. Strouse, *J. Am. Chem. Soc*. **2005**, *127*, 15791.
35. W. Xiong, G. Yang, X. Wu and J. Zhu, *ACS Appl. Mater. Interfaces* **2013**, *5*, 8210.
36. D. Zhao, Z. He, W. H. Chan, M. M. F. Cho, *J. Phys. Chem. C* **2009**, *113*, 1293.
37. T. Watanabe, K. Takahashi, K. Shimura, H. Bu, H.-D. Kim, and D. Kim, *Bull. Chem. Soc. Jpn.* **2017**, *90*, 52.
38. H. Bu, H. Kikunaga, K. Shimura, K. Takahasi, T. Taniguchi, and D. Kim, *Phys. Chem. Chem. Phys*. **2013**, *15*, 2903.
39. Y.-S. Lee, H. Bu, T. Taniguchi, T. Takagi, S. Sobue, H. Yamada, T. Iwaki, and D. Kim, *Chem. Lett*. **2016**, *45*, 878.
40. Y.-S. Lee, K. Nakano, H-B. Bu, and D. Kim, *Appl. Phys. Express.* **2017**, *10*, 065001.
41. H. Bu, H. Yokota, K. Shimura, T. Taniguchi, and D. Kim, *Chem. Lett*. **2015**, *44*, 200.
42. D. Kim, H. Yokota, T. Taniguchi, and M. Nakayama, *J. Appl. Phys*. **2013**, *114*, 154307.
43. B. Chen, H. Zhong, W. Zhang, Z. Tan, Y. Li, C. Yu, T. Zhai,Y. Bando, S. Yang and B. Zou, *Adv. Funct. Mater*. **2012**, *22*, 2081.
44. Z. Fang, Y. Li, H. Zhang, X. Zhong, and L. Zhu, *J. Phys. Chem. C* **2009**, *113*, 14145.
45. D. Zhao, J.-T. Li, F. Gao, C. Zhang, and Z. He, *RSC Adv*. **2013**, *4*, 47005.
46. K. T. Shimizu, W. K. Woo, B. R. Fisher, H. J. Eisler, and M. G. Bawendi, *Phys. Rev. Lett*. **2002**, *89*, 11741.
47. V. K. Komarala, Y. P. Rakovich, A. L. Bradley, S. J. Byrne, Y. K. Gun'ko, N. Gaponik, and A. Eychmüller, *Appl. Phys. Lett*. **2006**, *89*, 253118.
48. Y. Ito, K. Matsuda, and Y. Kanemitsu, *Phys. Rev. B* **2007**, *75*, 033309.
49. T. Pons, I. L. Medintz, K. E. Sapsford, S. Higashiya, A. F. Grimes, D. S. English, and H. Mattoussi, *Nano Lett* **2007**, *7*, 3157.
50. A. O. Govorov, J. Lee, and N. A. Kotov, *Phys. Rev. B* **2007**, *76*, 125308.
51. M. Lunz, V. A. Gerard, Y. K. Gun'ko, V. Lesnyak, N. Gaponik, A. S. Susha, A. L. Rogach, and A. L. Bradley, *Nano Lett.* **2011**, *11*, 3341.

Supporting Information

Synthesis of water-soluble $CuInS_2$ quantum dots by a hydrothermal method and their optical properties

Kazutaka Iida, Yota Uehigashi, Hideki Ichida, Hang-Beom Bu, and DaeGwi Kim*

Department of Applied Physics, Graduate School of Engineering, Osaka City University

3-3-138, Sugimoto, Sumiyoshi-ku, Osaka 558-8585, Japan

Figure S1 shows PL-decay profiles of the monolayer structure of CIS QDs and the bilayer structures of n = 0 and 8.

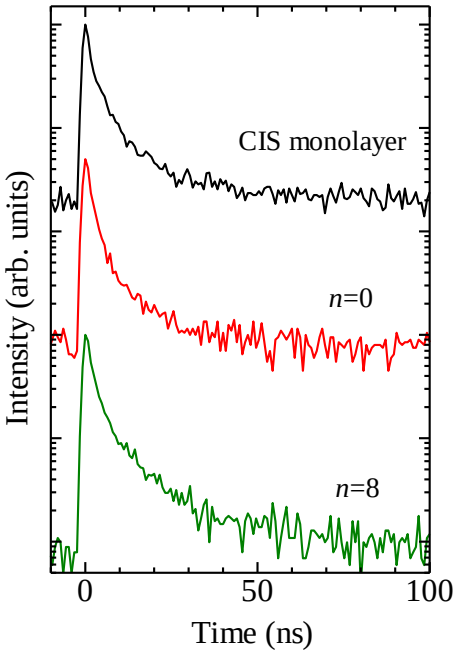

Fig. S1. PL-decay profiles of the monolayer structure of CIS QDs and the bilayer structures of n = 0 and 8.